Hindawi Publishing Corporation
Advances in High Energy Physics
Volume 2015, Article ID 967474, 12 pages
http://dx.doi.org/10.1155/2015/967474

Review Article

Properties of Full Jet in High-Energy Heavy-Ion Collisions from Parton Scatterings

Guo-Liang Ma[1] and Mao-Wu Nie[1,2]

[1] *Shanghai Institute of Applied Physics, Chinese Academy of Sciences, Shanghai 201800, China*
[2] *University of Chinese Academy of Sciences, Beijing 100049, China*

Correspondence should be addressed to Guo-Liang Ma; glma@sinap.ac.cn

Received 9 July 2014; Revised 2 October 2014; Accepted 4 November 2014

Academic Editor: Edward Sarkisyan-Grinbaum

Copyright © 2015 G.-L. Ma and M.-W. Nie. This is an open access article distributed under the Creative Commons Attribution License, which permits unrestricted use, distribution, and reproduction in any medium, provided the original work is properly cited. The publication of this article was funded by SCOAP[3].

The properties of fully reconstructed jet are investigated in p + p and Pb + Pb collisions at $\sqrt{s_{NN}}$ = 2.76 TeV within a multiphase transport (AMPT) model with both partonic scatterings and hadronic rescatterings. A large transverse momentum (p_T) asymmetry of dijet or photon-jet arises from the strong interactions between jet and partonic matter. The ξ-dependent jet fragmentation function in Pb + Pb collisions is decomposed into two contributions from different jet hadronization mechanisms, that is, fragmentation versus coalescence. The medium modification of differential jet shape displays that the jet energy is redistributed towards a larger radius owing to jet-medium interactions in heavy-ion collisions. Jet triangular azimuthal anisotropy coefficient, v_3^{jet}, which shows a smaller magnitude than the elliptic coefficient v_2^{jet}, decreases more quickly with increasing jet p_T, which can be attributed to a path-length effect of jet energy loss. All of these properties of full jet are consistent with the jet energy loss mechanism in a stronglyinteracting partonic matter in high-energy heavy-ion collisions.

1. Introduction

Plenty of experimental data from the BNL Relativistic Heavy Ion Collider (RHIC) and the CERN Large Hadron Collider (LHC) have confirmed that a nearly perfect fluid of strongly interacting quark-gluon plasma (QGP) could be created in the early state of high-energy heavy-ion collisions [1–4]. The origin and properties of this almost perfect-fluid QGP are the main subjects of heavy-ion collision studies. Jet, produced by initial hard processes, serves as an important probe to understand the properties of the QGP, since it loses its energy when it passes through the hot partonic medium, the effect which is called jet quenching [5]. The nuclear modification factor R_{AA}, which is the yield ratio of nucleus + nucleus collisions to inelastic p + p collisions normalized by the number of binary inelastic nucleon + nucleon collisions, shows a strong suppression at high transverse momentum p_T in central nucleus + nucleus collisions at the RHIC [6] and LHC [7] energies. The disappearance of away-side peak in dihadron azimuthal correlation presents the picture that the away-side jet is strongly suppressed by the QGP in central Au + Au collisions at the top RHIC energy [8]. On the other hand, the recent LHC measurements on fully reconstructed jets provide a comprehensive characterization of jet quenching. For instance, a larger dijet p_T asymmetry has been observed in central Pb + Pb collisions than in p + p collisions at the LHC energy [9, 10]. Since photon does not strongly interact with the QGP, the photon + jet measurements from CMS and ATLAS provide direct and less biased quantitative measures of jet energy loss in the medium, which give a deceasing jet-to-photon momentum imbalance ratio ($x_{j\gamma}$) from peripheral to central centrality bin in Pb + Pb collisions [11, 12]. The LHC measurements of the modification ratio of jet fragmentation function in Pb + Pb collisions to that in p + p collisions show the interesting features of no modification at low $\xi = \ln(1/z)$, a suppression at intermediate ξ, and an enhancement at high ξ for associated charged hadrons inside the jet cone [13–15]. The experimental results about differential jet shape show no modification at a small radius but a large enhancement at a large radius in

central Pb + Pb collisions, relative to that in p + p collisions [14, 16]. The data on the elliptic anisotropy of reconstructed jets from the ATLAS Collaboration show nonzero v_2 values for the jet p_T range from 45 to 160 GeV/c for all centrality bins in Pb + Pb collisions [17].

The current theoretical understandings of jet quenching consist of multiple approaches, which included both weak-coupling approaches based on perturbative QCD (pQCD) [18] and strong-coupling approaches based on anti-de Sitter space/conformal field theory (AdS/CFT) conjecture [19–21].

In this review, the properties of reconstructed jets are presented for p + p and Pb + Pb collisions at $\sqrt{s_{NN}} = 2.76$ TeV by using a multiphase transport (AMPT) model, which includes both dynamical evolutions of partonic scatterings and hadronic rescatterings. For partonic scatterings, the AMPT model uses an elastic cross section calculated from the pQCD. Several theoretical results are achieved in our numerical simulations. (i) A large p_T asymmetry of dijet or photon-jet is produced by strong interactions between jets and partonic matter [22, 23]. (ii) The measured jet fragmentation function ratio of Pb + Pb collisions to p + p collisions is decomposed into two parts, corresponding to the two contributions of jet hadronization from fragmentation and coalescence [24]. (iii) The differential jet shapes are significantly modified by the strong interactions between jets and the partonic medium in Pb + Pb collisions relative to that in p + p collisions [25]. (iv) Jet v_2 be in a good agreement with the recent ATLAS data and let jet v_3, which has a smaller magnitude than jet v_2, decrease quickly with the increasing of jet transverse momentum [26]. All of these features support a picture of jet energy loss in a strongly interacting partonic matter.

The review is organized as follows. In Section 2, we give a brief description of AMPT model. The basic mechanisms related to jet in the AMPT model are stated in Section 3. The analysis method for jet reconstruction is explained in Section 4. Results and discussions are presented for dijet, photon-jet, jet fragmentation function, jet shape, and jet azimuthal anisotropy in Section 5. Finally a summary is given in Section 6.

2. The AMPT Model

The AMPT model with a string melting scenario [27], which has well described many experimental observables [27–33], is implemented in this work. The AMPT model includes four main stages of high-energy heavy-ion collisions: the initial condition, parton cascade, hadronization, and hadronic rescatterings. The initial condition, which includes the spatial and momentum distributions of minijet partons and soft string excitations, is obtained from HIJING model [34, 35]. Then the strings are melted into quarks, and thus a quark and antiquark plasma are formed and start to evolve. The parton cascade process is simulated by Zhang's parton cascade (ZPC) model [36], where the partonic cross section is an elastic cross section controlled by the value of strong-coupling constant α_s and the Debye screening mass μ. The AMPT model recombines partons via a simple coalescence model to produce hadrons when the partons freeze out. The dynamics of the subsequent hadronic rescatterings is then described by a relativistic transport (ART) model [37].

In this work, the AMPT model with the newly fitted parameters (such as $\alpha_s = 0.33$ and $\mu = 3.2\,\mathrm{fm}^{-1}$, which corresponds to a parton interaction cross section $\sigma = 1.5$ mb, and parameters $a = 0.9$ and $b = 0.5\ \mathrm{GeV}^2$ in the Lund string fragmentation model) is used to simulate Pb + Pb collisions at $\sqrt{s_{NN}} = 2.76$ TeV. It has shown good descriptions for many experimental observables at the LHC energy, such as pseudorapidity and p_T distributions [38], and harmonic flows [39, 40]. Two sets of Pb + Pb simulations are performed by setting the partonic interaction cross section as 1.5 or 0 mb, which corresponds to two different physical scenarios for partonic + hadronic interactions and hadronic interactions only, respectively.

3. Jet in the AMPT Model

Because the jet production cross section with large transverse momentum is very small, the dijet or photon-jet (denoted as γ-jet) production is triggered in the initial condition of the HIJING model, which requires that each event has a dijet or γ-jet with a specified p_T, in order to increase the simulation efficiency. Several hard QCD processes are taken into account for the initial dijet production with the jet triggering technique in the HIJING model [34, 35], which includes $q_1 + q_2 \to q_1 + q_2$, $q_1 + \overline{q_1} \to q_2 + \overline{q_2}$, $q + \overline{q} \to g + g$, $q + g \to q + g$, $g + g \to q + \overline{q}$, and $g + g \to g + g$, with consideration of initial- and final-state radiation corrections. Three prompt photon production processes are taken into account for the γ-jet study, including $q + \overline{q} \to g + \gamma$, $q + \overline{q} \to \gamma + \gamma$, and $q + g \to q + \gamma$ [41]. The high-p_T primary partons evolve into jet showers full of lower virtuality partons through initial- and final-state QCD radiations. In the string melting mechanism, all excited strings and jets are fragmented into hadrons according to the Lund string fragmentation. Then these hadrons are converted to quarks according to the flavor and spin structures of their valence quarks. After the melting process, the jet parton showers are converted into clusters of on-shell constituent quarks and antiquarks, and a plasma of on-shell constituent quarks and antiquarks is also formed. Next, the jet transport is simulated by the ZPC model including all possible elastic partonic interactions among the medium quarks and jet shower quarks, but without including inelastic parton interactions or further radiations at present. It means that our simulations currently do not include the mechanism of jet radiation energy loss. However a large partonic interaction cross section can partially play an effective role, and we expect to improve it by including many-body interactions into the process of parton cascade in the future. When the quarks freeze out, they are recombined into medium hadrons or jet shower hadrons via a simple coalescence model which combines two nearest quark and antiquark into a meson and three nearest quarks into a baryon. The final-state hadronic interactions, including elastic and inelastic scatterings between jet and hadrons and resonance decays, can be automatically described by the ART model.

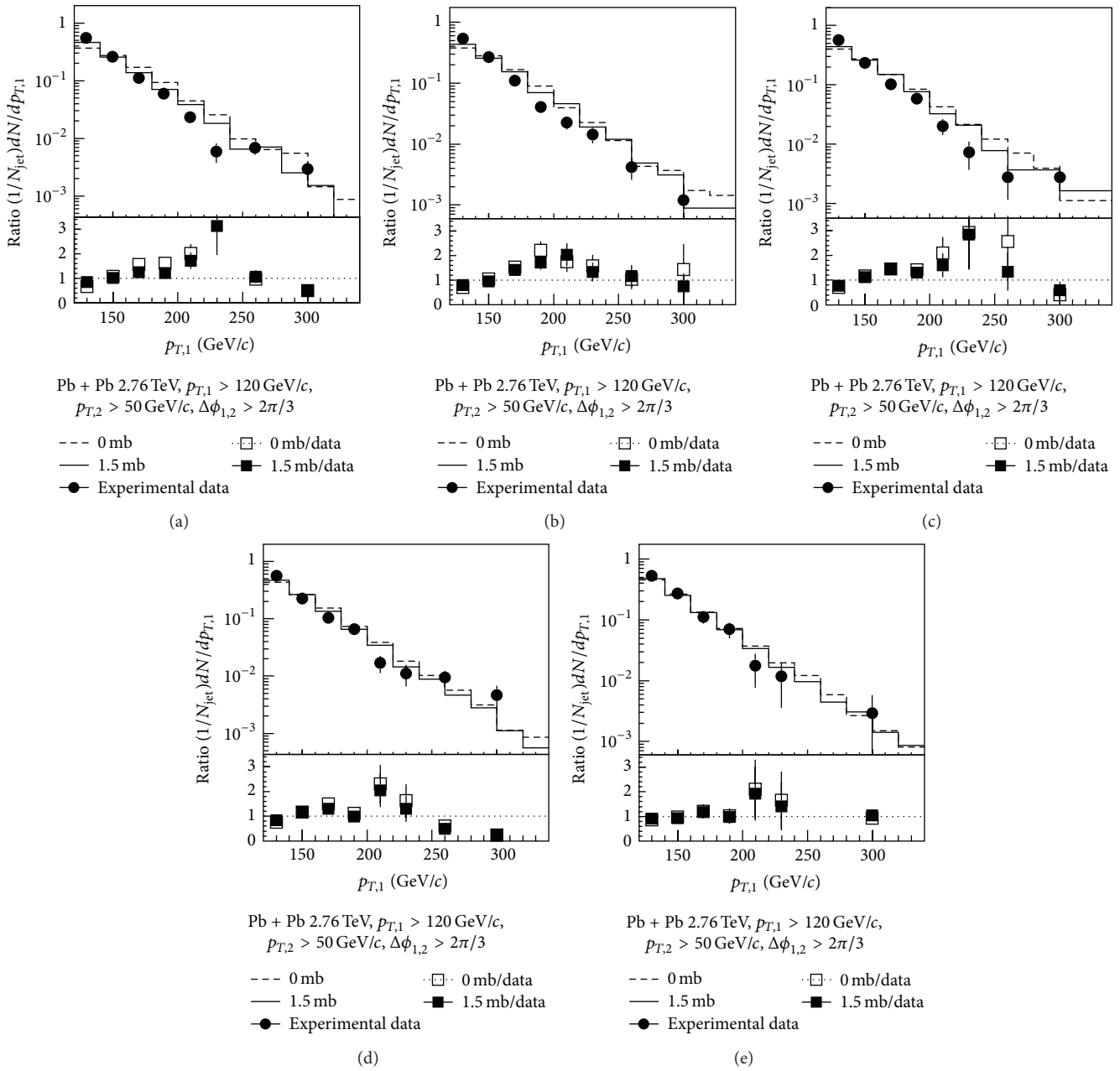

FIGURE 1: Leading jet p_T distributions for dijet events with subleading jets of $p_{T,2} > 50$ GeV/c in Pb + Pb collisions at $\sqrt{s_{NN}} = 2.76$ TeV for five centrality bins: (a) 0–10%, (b) 10–20%, (c) 20–30%, (d) 30–50%, and (e) 50–100%, where the solid (1.5 mb) and dash (0 mb) histograms represent the AMPT results with partonic + hadronic interactions and hadronic interactions only, respectively, while the solid circles represent the data from the CMS experiment [10]. The lower part in each panel depicts the ratios of AMPT results to experimental data.

4. Jet Reconstruction

An anti-k_t algorithm from the standard Fastjet package is used to reconstruct full jets [42]. The kinetic cuts of reconstructed jet, such as the jet cone size R and jet p_T, are always chosen to be consistent with the CMS or ATLAS experiment, which will be used for each analysis in the next section. It is very important to remove the underlying event background from the raw reconstructed jet cleanly, since there are thousands of tracks produced in high-energy heavy-ion collisions. Two methods are applied for removing the background of reconstructed jets in our analyses. (i) A pseudorapidity strip of width $\Delta\eta = 1.0$ centered on the jet position, with two highest-energy jets excluded, is used to estimate the background ("average energy per jet area"), which is subtracted from the reconstructed jet energy. It is used to analyze dijet or γ-jet asymmetry and jet azimuthal anisotropy. (ii) The η-reflection method is used for reconstructing jet fragmentation function and differential jet shape, as the CMS experiment did. We select the particles that lie in a background jet cone obtained by reflecting the original jet cone around $\eta = 0$ while keeping the same ϕ

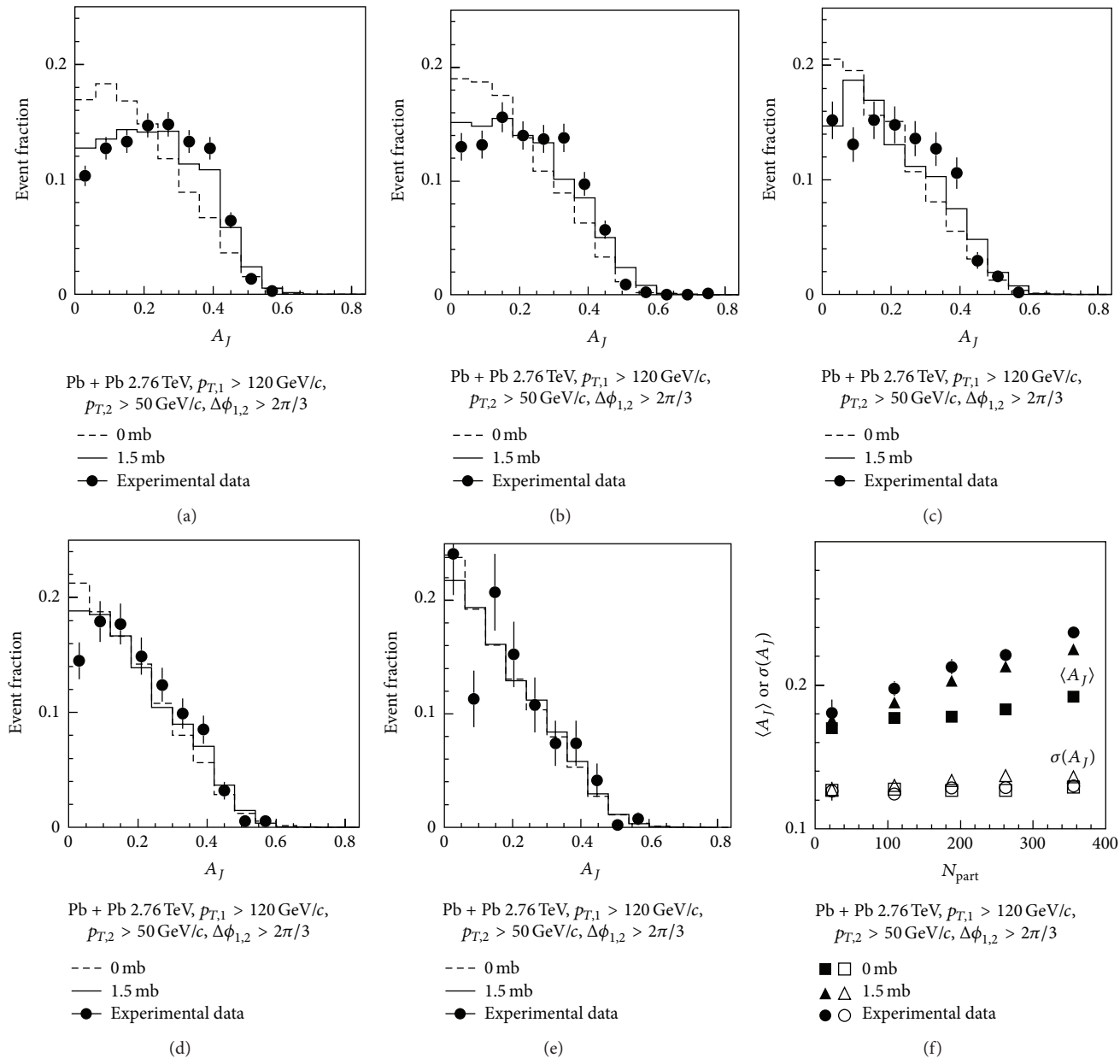

FIGURE 2: Dijet asymmetry ratio A_J distributions for leading jets of $p_{T,2} > 120$ GeV/c with subleading jets of $p_{T,2} > 50$ GeV/c and $\Delta\phi_{1,2} > 2\pi/3$ in Pb + Pb collisions at $\sqrt{s_{NN}} = 2.76$ TeV for five centrality bins: (a) 0–10%, (b) 10–20%, (c) 20–30%, (d) 30–50%, and (e) 50–100%, where the solid (1.5 mb) and dash (0 mb) histograms represent the AMPT results with partonic + hadronic and hadronic interactions only, respectively, while the solid circles represent the data from the CMS experiment [10]. (f) The mean values and variances of A_J distributions as functions of N_{part}.

coordinate. For each signal jet, the background distribution is subtracted from the raw distribution obtained from the jet cone. Jets in an η-strip region ($|\eta| < 0.3$) are excluded to avoid overlap between the signal jet region and the region used for background estimation.

5. Results and Discussions

5.1. Dijet. A dijet with $p_T \sim 120$ GeV/c is triggered in the dijet simulations. For the analysis cuts, the transverse momentum of leading jet is required to be larger than 120 GeV/c ($p_{T,1} > 120$ GeV/c), while that of subleading jet is required to be larger than 50 GeV/c ($p_{T,2} > 50$ GeV/c). The azimuthal angle between leading and subleading jets is larger than $2\pi/3$ ($\Delta\phi_{1,2} > 2\pi/3$), where the subscripts 1 and 2 refer to the leading jet and subleading jet, respectively [10]. Only jets within a midrapidity range of $|\eta_{1,2}| < 2$ are considered.

Figure 1 shows the leading jet p_T distributions in Pb + Pb collisions at $\sqrt{s_{NN}} = 2.76$ TeV for different centrality bins. Centrality in the AMPT model is defined by different

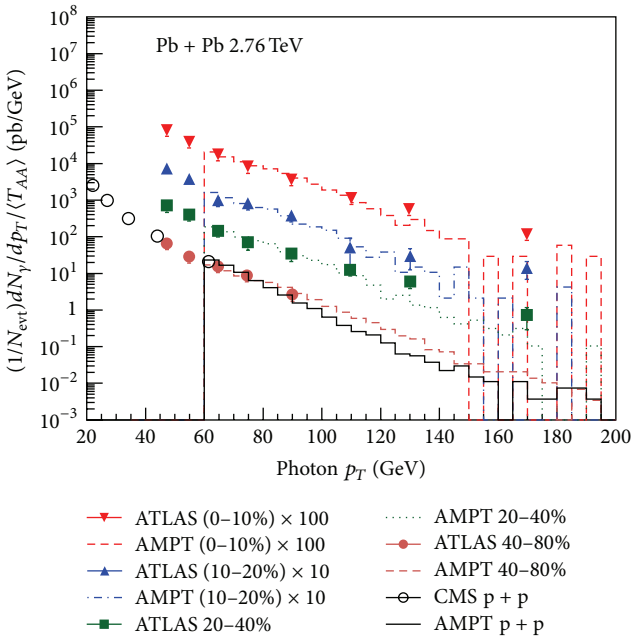

FIGURE 3: Transverse momentum spectra of prompt photons for 0–10%, 10–20%, 20–40%, and 40–80% Pb + Pb collisions (scaled by $1/T_{AA}$) and p + p collisions at 2.76 TeV, scaled by different factors for easier viewing, where the histograms represent the AMPT spectra, while the symbols represent the data from ATLAS [43] and CMS experiment [44].

ranges of impact parameters. The AMPT simulations with partonic + hadronic interactions (1.5 mb) present the spectra a little softer than those with hadronic interactions only (0 mb). Note that the measured leading jet p_T distributions have not been corrected for some detector effects such as detector resolution, fluctuations in and out of the jet cone, or underlying event fluctuations [10]. From a quantitative comparison of the ratios of AMPT results to experimental data (lower part in each panel of Figure 1), the AMPT model can reproduce the data to a good degree.

To characterise the transverse momentum balance (or imbalance) of dijet, an asymmetry ratio is defined as $A_J = (p_{T,1} - p_{T,2})/(p_{T,1} + p_{T,2})$ as LHC experiments did [9, 10]. The dijet asymmetry A_J distributions for different centrality bins are shown in Figures 2(a)–2(e). For more peripheral collisions, both sets of AMPT results give similar descriptions of the data, since the partonic interactions are relatively weak in peripheral collisions. However, it is different for more central collisions where the AMPT results with partonic + hadronic interactions give more asymmetric A_J distribution than those with hadronic interactions only. For instance, for the most central centrality bin (0–10%) in Figure 2(a), the AMPT results (1.5 mb) give a much better description than AMPT results (0 mb). Figure 2(f) presents the mean values $\langle A_J\rangle$ and variances $\sigma(A_J)$ of A_J distributions as functions of a number of participant nucleons, N_{part}. The AMPT results (1.5 mb) can well describe the two characteristic quantities for dijet A_J distributions simultaneously; however the AMPT results (0 mb) underestimate $\langle A_J\rangle$. This indicates that it is the strong interactions between the jets and the partonic matter that yield the observed large p_T imbalance between the two back-to-back jets.

5.2. Photon-Jet. A γ-jet of $p_T^\gamma \sim 60$ GeV/c is triggered in the γ-jet simulations. The kinetic cuts for the analysis on γ-jet transverse momentum imbalance are chosen to be consistent with the CMS experiment [11]. The transverse momentum of prompt photon is required to be larger than 60 GeV/c ($p_T^\gamma >$ 60 GeV/c) and its pseudorapidity is within a midrapidity gap of 1.44 ($|\eta^\gamma| < 1.44$). A jet cone size is set to be 0.3 ($R = 0.3$), p_T of jet is larger than 30 GeV/c ($p_T^{\text{jet}} > 30$ GeV/c), and pseudorapidity of jet is within a midrapidity range of $|\eta^{\text{jet}}| < 1.6$. After removing the underlying event background, the triggered γ-jet events are sampled, with the measured experimental prompt photon p_T spectra as the weight. Figure 3 shows the final p_T spectra of prompt photons in comparison with the ATLAS Pb + Pb [43] and CMS p + p data [44].

Compared with dijet, γ-jet have its unique advantage. Because the prompt photon has no strong interactions with medium, it can provide a natural calibration of initial jet energy. Therefore, the transverse momentum imbalance is defined as the ratio of $x_{j\gamma} = p_T^{\text{jet}}/p_T^\gamma$ to study jet energy loss mechanism [11, 12]. Figures 4(a)–4(d) show the imbalance ratio distributions for four centrality bins of Pb + Pb collisions and p + p collisions at $\sqrt{s_{NN}} = 2.76$ TeV. The AMPT results with both partonic and hadronic interactions (i.e., 1.5 mb) give a little smaller $x_{j\gamma}$ and $\langle x_{j\gamma}\rangle$ than those with hadronic interactions only (i.e., 0 mb) and experimental data. To quantitively learn how much jet loses its energy in partonic or hadronic matter, the averaged energy loss fraction of jet, $\langle \Delta p_T/p_T\rangle$, is checked but not shown here, which shows that jet loses its energy from by ~15% in central collisions down to by ~5% in peripheral collisions due to decreasing of partonic interactions, whereas hadronic interactions with vanished partonic interactions only can give much smaller energy loss fraction around 4%–2% [23]. It indicates that the strong interactions between jet parton shower and partonic matter can produce a larger momentum asymmetry than the interactions between jet hadron shower and hadronic matter, especially for more central collisions.

5.3. Jet Fragmentation Function. To acquire jet fragmentation functions, the kinetic cuts for jet reconstruction are chosen to be consistent with the CMS experiment [14]. The jet cone size is set to 0.3. The transverse momentum of jet is required to be larger than 100 GeV/c ($p_T > 100$ GeV/c) within a pseudorapidity range of $0.3 < |\eta| < 2$ for this analysis, where jets within $|\eta| < 0.3$ are excluded to avoid the overlap between the signal jet region and the jet background estimation region. The jet fragmentation function is obtained by correlating charged hadrons with $p_T > 1$ GeV/c falling within the jet cone, with respect to the axis of reconstructed jet. As the CMS experiment defined, the jet fragmentation function, $D(\xi) = 1/N_{\text{jet}} dN_{\text{ch}}/d\xi$, can be presented as a function of the variable $\xi = \ln(1/z)$, where $z = p_\parallel^{\text{ch}}/p^{\text{jet}}$ is the fraction of the jet energy carried by the charged particle, $p_\parallel^{\text{ch}}$ is the momentum component of charged particle along the jet axis, p^{jet} is the magnitude of reconstructed jet momentum,

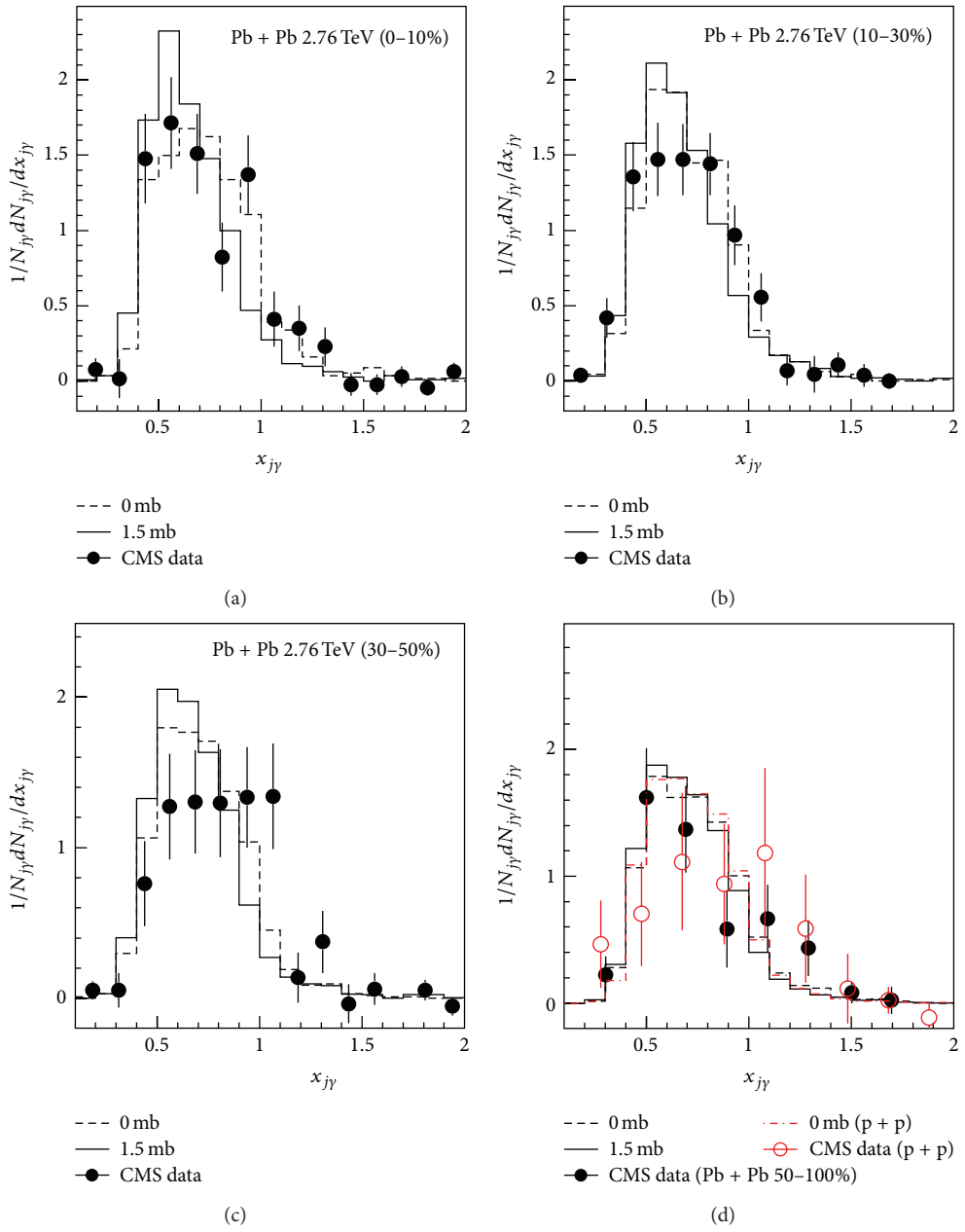

FIGURE 4: The distributions of imbalance ratio $x_{j\gamma} = p_T^{\text{jet}}/p_T^{\gamma}$ between the photon ($p_T^{\gamma} > 60$ GeV/c) and jet ($p_T^{\text{jet}} > 30$ GeV/c, $\Delta\phi_{j\gamma} > 7\pi/8$) after background subtraction for four centrality bins in Pb + Pb and p + p collisions, where the solid (1.5 mb) and dash (0 mb) histograms represent the AMPT results with partonic + hadronic and hadronic interactions only, respectively, while the circles represent the data from the CMS experiment [11].

and N_{jet} is the total number of jets. All charged particles in the cone of 0.3 around the jet axis are included in this analysis. It should be noted that lower ξ actually corresponds to higher p_T. An η-reflection method is used to estimate the background, which is subtracted from the reconstructed jet fragmentation function in Pb + Pb collisions.

Figure 5(a) shows the jet fragmentation function $D(\xi)$ in p + p collisions at $\sqrt{s_{NN}} = 2.76$ TeV. From a quantitative comparison of the ratio of AMPT result to experimental data shown in Figure 5(b), the result obtained from AMPT simulations with hadronic interactions can only basically describe the jet fragmentation function in p + p collisions, which provides a reliable baseline for the following studies in Pb + Pb collisions with the AMPT model with partonic + hadronic interactions.

Because heavy-ion collisions involve many important stages, the evolution of the jet fragmentation function during different stages can provide the important information about the mechanism of medium modifications of jet fragmentation functions in Pb + Pb collisions. Figure 6 presents the jet

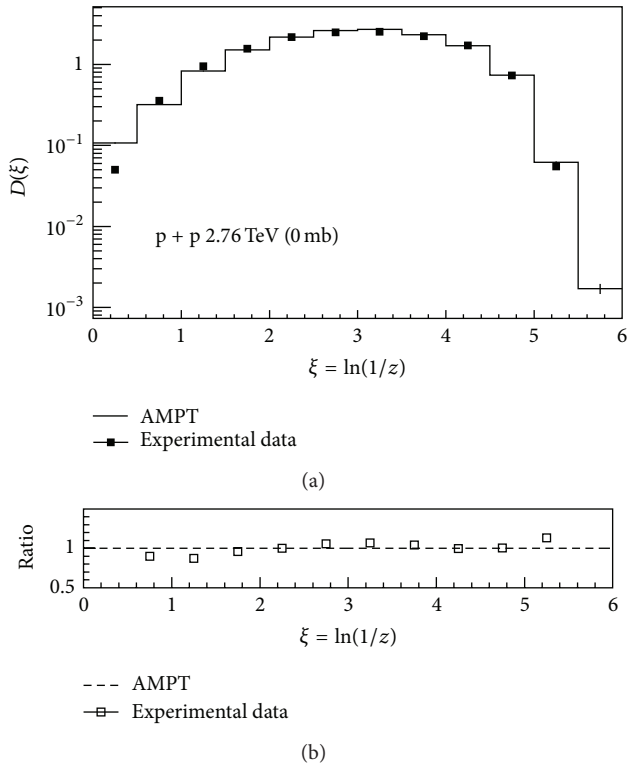

FIGURE 5: (a) The jet fragmentation function $D(\xi)$ in p + p collisions at $\sqrt{s_{NN}}$ = 2.76 TeV, where the histograms represent the AMPT (0 mb) result with hadronic interactions only and the squares represent the data from the CMS experiment [14]. (b) The ratio of AMPT result to experimental data.

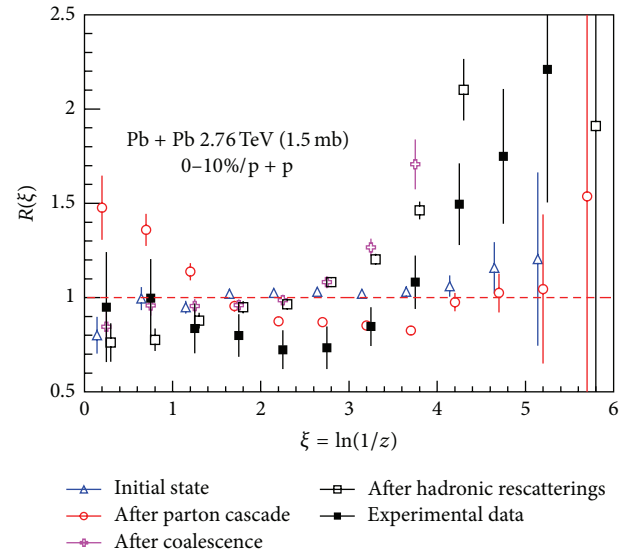

FIGURE 6: The jet fragmentation function ratios of the most central centrality bin (0–10%) in Pb + Pb collisions to p + p collisions at different evolution stages. The solid squares represent the data from the CMS experiment [14]. Some points are slightly shifted along the x-axis for better representation.

fragmentation function ratios of the most central events (0–10%) in Pb + Pb collisions to p + p collisions; that is, $R(\xi) = D_{\mathrm{Pb+Pb}}(\xi)/D_{\mathrm{p+p}}(\xi)$, at different evolution stages from AMPT simulations with partonic + hadronic interactions (1.5 mb). Some points are slightly shifted along the x-axis for better representation. The initial jet fragmentation function ratio is around unity which indicates no modification in the initial state of Pb + Pb collisions. Two basic features of modification, an enhancement at low ξ and a suppression at intermediate ξ, appear in the jet fragmentation function ratio after the process of parton cascade. The enhancement at low ξ area is due to the fact that the energy loss of the jet is more significant than that of leading-like partons, which relatively decrease their ξ. On the other hand, the suppression is the result of the decrease of associated particles with intermediate p_T owing to the jet energy loss in the partonic medium, which are probably shifted to lower p_T or even thermalized. However, the expected high-ξ enhancement owing to the shift or thermalization is hard to be seen for the current statistics. A significant enhancement around intermediate and high ξ and small suppression at low ξ are observed after coalescence. It is because the coalescence mechanism in the AMPT slightly increases the total momentum of jet, owing to the involution of medium partons, and also increases the momenta of shower hadrons in comparison with the previous stage. And there is little effect from hadronic rescatterings. However, neither of the final jet fragmentation function ratios in the simulations can fit the experimental data for the whole ξ range.

The reason why the AMPT results can not match the measured jet fragmentation function ratio for the whole ξ range is that the AMPT model with a string-melting scenario only uses a coalescence model for hadronization but misses the other important one, that is, fragmentation. Actually, the interplay of fragmentation and coalescence indeed can give very good descriptions such as p_T spectra and elliptic flow in a wide p_T range [45]. To well describe the experimental data of the jet fragmentation function ratio in the whole ξ range, it is proposed to decompose the measured jet fragmentation function ratio to

$$R(\xi) = \lambda_f R_f(\xi) + \lambda_c R_c(\xi), \quad (1)$$

where $\lambda_f R_f(\xi)$ and $\lambda_c R_c(\xi)$ are fragmentation and coalescence parts, respectively, which are assumed to coexist in the measured jet fragmentation function ratio $R(\xi)$. λ_f and λ_c are the contribution factors for fragmentation and coalescence parts, respectively. The functional form of $R_f(\xi)$ is assumed to be the same as that of jet fragmentation function ratio after parton cascade, based on the parton-hadron duality or the subleading correction effect of fragmentation on the nuclear modification factor [46]. The functional form of $R_c(\xi)$ is assumed to be equal to the jet fragmentation function ratio after hadronic rescatterings, which includes both effects of coalescence and hadronic rescatterings. Thus, the two contribution parts can be obtained by fitting the experimental data of $R(\xi)$ with (1). It should be noted that λ_f and λ_c are assumed to be independent of ξ for simplicity in this work, which also can be understood as averaged values.

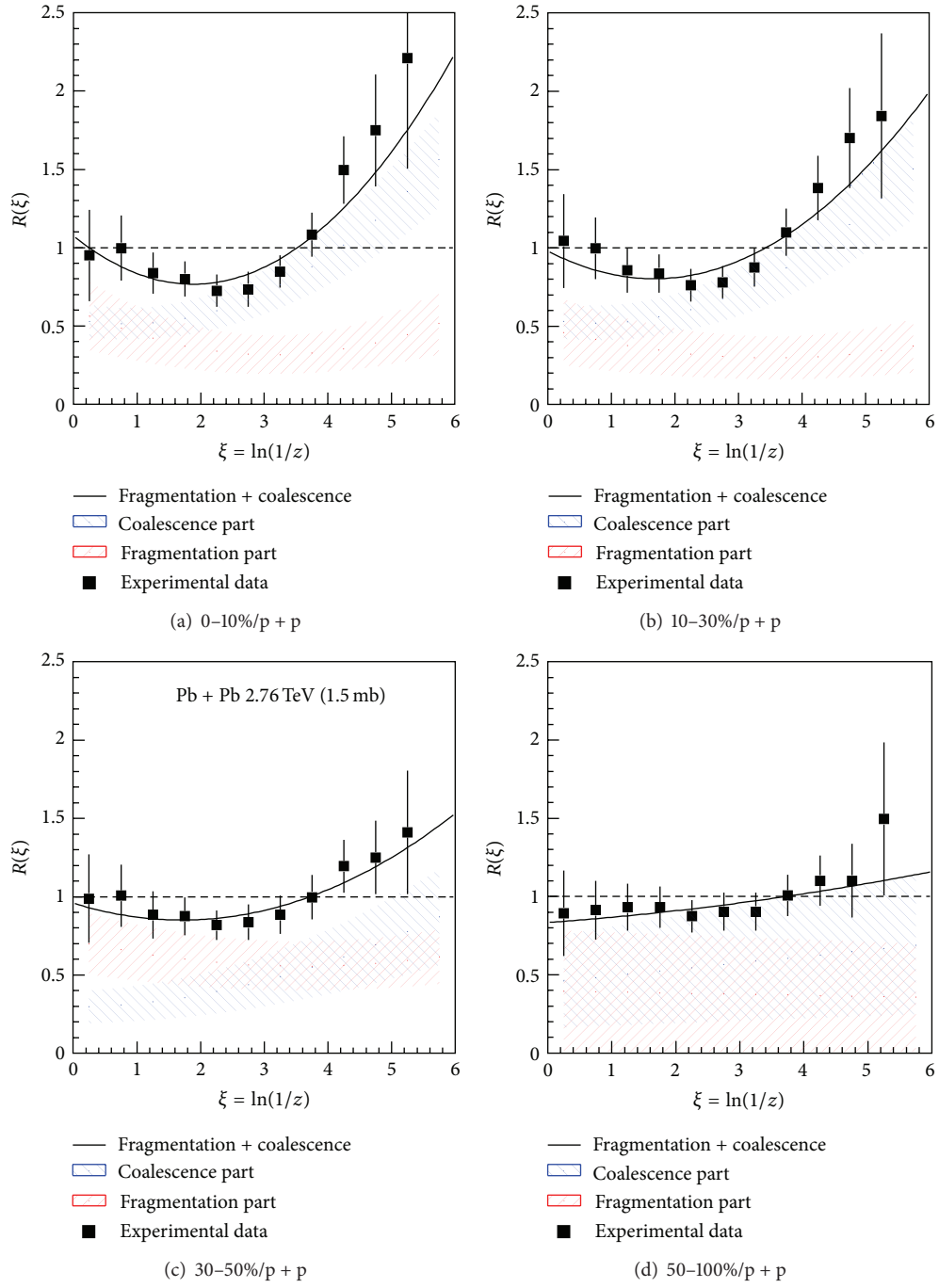

FIGURE 7: The jet fragmentation function ratios of four centrality bins in Pb + Pb collisions to p + p collisions. The solid curves show two-component (fragmentation + coalescence) fitting functions, while the two kinds of hatched areas give the fragmentation and coalescence contribution parts, that is, $\lambda_f R_f(\xi)$ and $\lambda_c R_c(\xi)$, for the jet fragmentation function ratios measured by the CMS experiment [14].

The solid curves in Figures 7(a)–7(d) show the combined fits to the measured jet fragmentation function ratios of different centrality bins in Pb + Pb collisions to p + p collisions with (1). From the fits, the two contributions from fragmentation and coalescence, $\lambda_f R_f(\xi)$ and $\lambda_c R_c(\xi)$, respectively, are shown by different kinds of hatched areas for which their uncertainties are mainly controlled by the errors of experimental data and the AMPT results. For more central collisions in Figures 7(a) and 7(b), the contribution from coalescence is much larger than that from fragmentation in the high-ξ range. With decreasing ξ, the contribution from coalescence drops down quickly while the contribution from fragmentation seems unchanged, until the two contributions become similar in the very low-ξ range. However, it is different for the mid-central collisions in Figure 7(c), which shows two similar contributions in the high-ξ range and

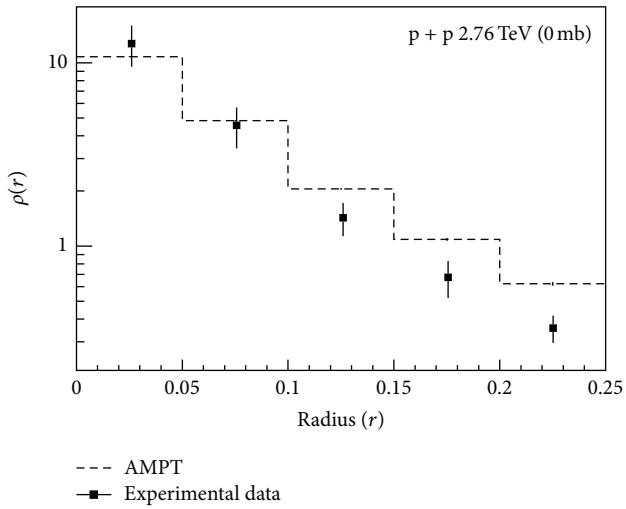

FIGURE 8: The differential jet shapes $\rho(r)$ in p + p collisions at $\sqrt{s_{NN}}$ = 2.76 TeV, where the histogram represents the AMPT result with hadronic interactions only and the squares represent the data from the CMS experiment [14, 16].

a dominant contribution from fragmentation in the low-ξ range. For the most peripheral collisions in Figure 7(d), it is hard to conclude due to the large uncertainties of two contributions. In general, the effect of coalescence tends to be more dominant for the high-ξ range in more central collisions, while the contribution from fragmentation becomes more important for the low-ξ range in more peripheral collisions.

5.4. Jet Shape. To reconstruct jet shape, the kinematic cuts are chosen to be consistent with the CMS experiment [14, 16]. The transverse momentum of a jet is required to be larger than 100 GeV/c within a pseudorapidity η range of $0.3 < |\eta| < 2$ for this analysis. Jets within $|\eta| < 0.3$ are excluded in order to avoid the overlap between the signal jet region and the jet background estimation region. The jet cone sizes R are set to be 0.3. The differential jet shape $\rho(r)$ is defined as the fraction of the transverse momentum carried by particles ($p_T > 1$ GeV/c) associated with the jet, which are contained inside an (η, ϕ (azimuthal angle)) annulus of inner and outer radii of $r \pm \delta r/2$ around the jet axis, where δr is chosen to be 0.05 and $0 \le r \le R$. $\rho(r)$ satisfies the normalization condition $\int_0^R \rho(r)dr = 1$. The η-reflection method is used to estimate the background, which is subtracted from the reconstructed differential jet shape.

Figure 8 shows the comparison of the differential jet shapes $\rho(r)$ between the AMPT result with hadronic interactions only (0 mb) and the experimental data for p + p collisions at $\sqrt{s_{NN}}$ = 2.76 TeV. The AMPT result basically can describe p + p data, which provides a qualified baseline for the following calculations in Pb + Pb collisions.

Figures 9(a)–9(d) present the differential jet shape ratios of different centrality bins in Pb + Pb collisions to p + p collisions from AMPT simulations with hadronic interactions only (0 mb) and with both partonic and hadronic interactions (1.5 mb), in comparisons with the experimental data. Some points are slightly shifted along the x-axis for better representation. It is found that including only hadronic interactions between jets and hadronic medium can hardly modify the energy distributions of reconstructed jets for all centrality bins in Pb + Pb collisions. On the other hand, the AMPT results with both partonic and hadronic interactions give relatively larger modifications, which indicates that the observed medium modifications of differential jet shapes mainly result from the interactions between jets and partonic medium. The emergent modifications in central Pb + Pb collisions show a suppression at a small radius and an enhancement at a large radius, which implies that the jet energy is redistributed towards a larger radius via the strong interactions between jet and the partonic medium.

5.5. Jet Azimuthal Anisotropy. To reconstruct jet azimuthal anisotropy, the kinematic cuts are chosen to be the same as those in the ATLAS experiment [17]. The jet cone size R is set to be 0.2. The average energy per jet area, as the underlying event background, is subtracted from the reconstructed jet energy in Pb + Pb collisions. Only jets within a midrapidity range of $|\eta| < 2$ are considered in this analysis.

It is well known that all orders of harmonic flows can arise from the initial geometry fluctuations through final-state interactions [47, 48]. Futhermore, the even orders of harmonic flows can be affected by initial fluctuations in the collision geometry [49]. To calculate the nth Fourier coefficient of jets v_n^{jet}, the nth event plane Ψ_n^r can be defined as

$$\Psi_n^r = \frac{1}{n}\left[\arctan\frac{\langle r^n \sin(n\varphi)\rangle}{\langle r^n \cos(n\varphi)\rangle} + \pi\right], \tag{2}$$

where r and φ are the coordinate position and azimuthal angle of each parton in the AMPT initial state and the average $\langle\cdots\rangle$ denotes density weighting. Then v_n^{jet} can be obtained from the following equation:

$$v_n^{\text{jet}} = \left\langle \cos\left[n\left(\phi^{\text{jet}} - \Psi_n^r\right)\right]\right\rangle. \tag{3}$$

Note that although the definition for v_n^{jet} is the same as that for a single hadron, it is, however, expected to have a smaller bias because the reconstructed jet has kinematic properties that are more closely related to those of the parent partons [17].

Jets v_2 and v_3 as a function of N_{part} for two typical p_T bins of $45 < p_T < 60$ GeV/c and $60 < p_T < 80$ GeV/c, calculated by (2) and (3) and denoted as $v_2^{\text{jet}}\{\Psi_2^r\}$ and $v_3^{\text{jet}}\{\Psi_3^r\}$, are shown in Figures 10(a) and 10(b), respectively. $v_2^{\text{jet}}\{\Psi_2^r\}$ (open triangles) is consistent with the jet v_2 calculations of $v_2^{\text{jet}}\{\Psi_n^r\}$ (open circles), though it has a little higher magnitudes due to the initial fluctuation contribution [49]. For jet v_3, it is smaller than jet v_2. By comparing jet v_3 between two different jet p_T bins, jet v_3 tends to vanish with the increase of jet p_T. On the other hand, we checked that the jet passes a longer path length through the medium in the direction of $\Delta\phi \sim \pi/2$ or $\Delta\phi \sim \pi/3$ for an elliptic or triangle shape profile, which is consistent with the path-length effect of jet energy loss [50].

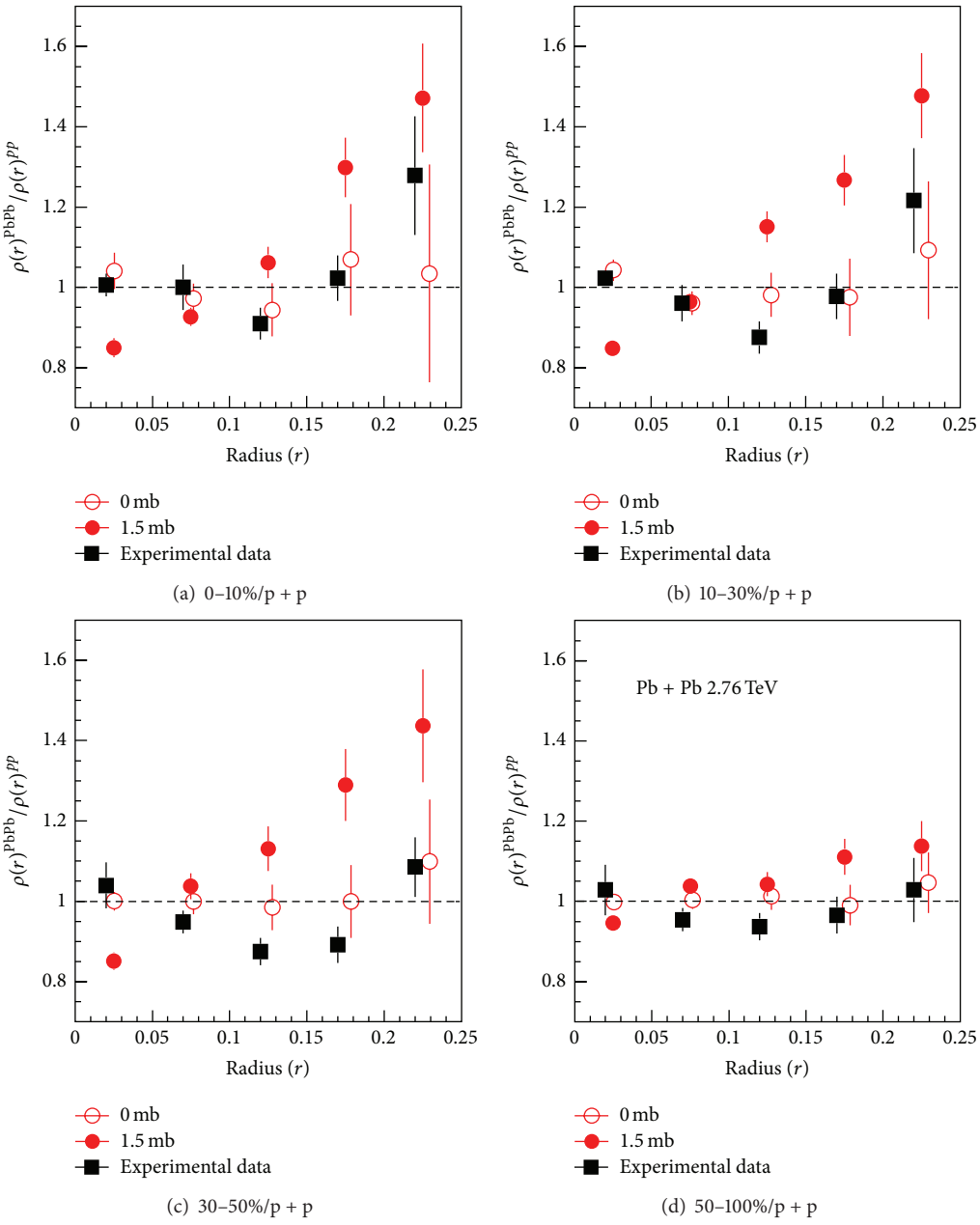

FIGURE 9: The differential jet shape ratios of four centrality bins in Pb + Pb collisions to p + p collisions, where solid circles represent the AMPT results with partonic + hadronic interactions (1.5 mb), open circles represent the AMPT results with hadronic interactions only (0 mb), and solid squares represent the data from the CMS experiment [14]. Some points are slightly shifted along the x-axis for better representation.

6. Summary

In summary, the properties of fully reconstructed jet are investigated within the AMPT model with both elastic partonic scatterings and hadronic rescatterings. A large p_T asymmetry of dijet or photon-jet is produced by the strong interactions between jets and partonic matter. These partonic scatterings lead to medium modifications of full jets in Pb + Pb collisions with respect to p + p collisions. The measured jet fragmentation function ratio of Pb + Pb collisions to p + p collisions, which depends on $\xi = \ln(1/z)$, can be decomposed into two contributions of jet hadronization from fragmentation and coalescence. The medium modification of differential jet shape indicates that the jet energy is redistributed towards a larger radius through the strong scatterings between jet and the partonic medium. A jet azimuthal anisotropy coefficient v_2^{jet} is in good agreement with the recent ATLAS data. v_3^{jet} has a smaller magnitude than v_2^{jet} and decreases quickly with increasing jet p_T, owing to the path-length effect of jet energy loss. The properties of full jet in Pb + Pb collisions disclose the fact that jet loses energy

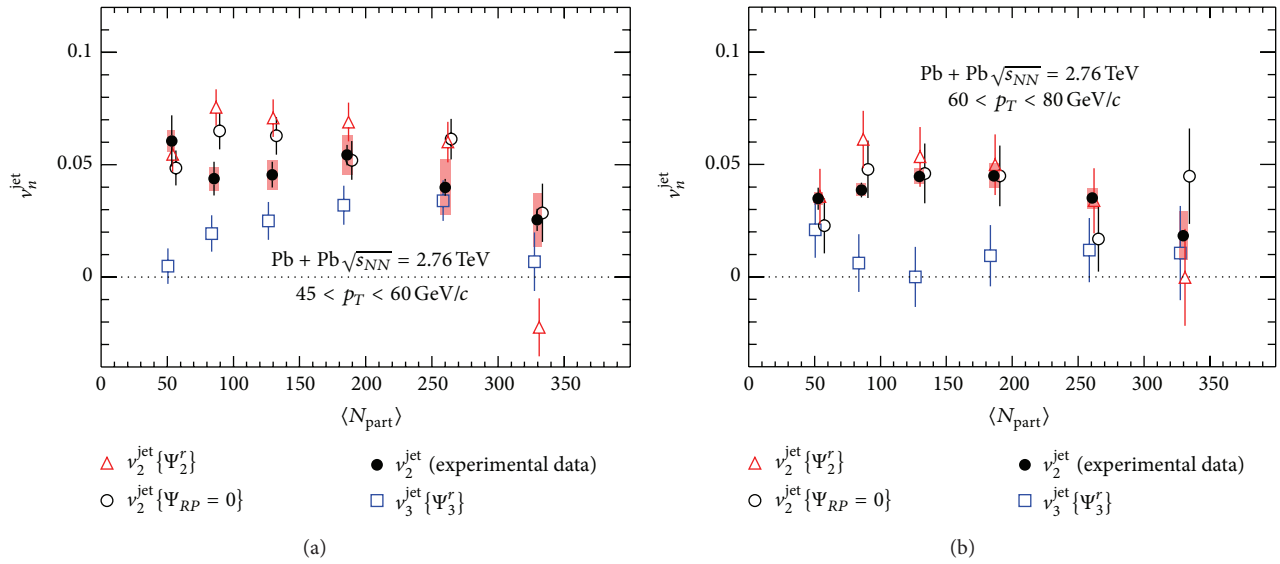

FIGURE 10: v_n^{jet} (n = 2 and 3) as a function of N_{part} for jet p_T bins of 45 < p_T < 60 GeV/c (a) and 60 < p_T < 80 GeV/c (b) in Pb + Pb collisions at $\sqrt{s_{NN}}$ = 2.76 TeV, where open triangles represent v_2^{jet} with respect to Ψ_2^r, open circles represent v_2^{jet} with respect to $\Psi_{RP} = 0$, open squares represent v_3^{jet} with respect to Ψ_3^r, and solid circles represent the ATLAS experimental data [17]. Some points are slightly shifted along the x-axis for better representation.

through the strong interactions between jet and the hot and dense partonic matter in high-energy heavy-ion collisions.

Conflict of Interests

The authors declare that there is no conflict of interests regarding the publication of this paper.

Acknowledgments

This work was supported by the Major State Basic Research Development Program in China under Grant no. 2014CB845404, the NSFC under Grant nos. 11175232, 11035009, 11375251, and 11421505, the Knowledge Innovation Program of CAS under Grant no. KJCX2-EW-N01, and the CCNU-QLPL Innovation Fund under Grant no. QLPL2011P01.

References

[1] J. Adams, M. M. Aggarwala, Z. Ahammed et al., "Experimental and theoretical challenges in the search for the quark-gluon plasma: the STAR Collaboration's critical assessment of the evidence from RHIC collisions," *Nuclear Physics A*, vol. 757, no. 1-2, pp. 102–183, 2005.

[2] K. Adcox, S. S. Adler, S. Afanasiev et al., "Formation of dense partonic matter in relativistic nucleus-nucleus collisions at RHIC: experimental evaluation by the PHENIX Collaboration," *Nuclear Physics A*, vol. 757, no. 1-2, pp. 184–283, 2005.

[3] B. Müller, J. Schukraft, and B. Wysłouch, "First results from Pb+Pb collisions at the LHC," *Annual Review of Nuclear and Particle Science*, vol. 62, pp. 361–386, 2012.

[4] G. Roland, K. Šafařík, and P. Steinberg, "Heavy-ion collisions at the LHC," *Progress in Particle and Nuclear Physics*, vol. 77, pp. 70–127, 2014.

[5] X.-N. Wang and M. Gyulassy, "Gluon shadowing and jet quenching in $A + A$ collisions at $\sqrt{s_{NN}}$ = 200A GeV," *Physical Review Letters*, vol. 68, no. 10, pp. 1480–1483, 1992.

[6] J. Adams, C. Adler, M. M. Aggarwal et al., "Transverse momentum and collision energy dependence of high p_T hadron suppression in Au+Au collisions at ultrarelativistic energies," *Physical Review Letters*, vol. 91, no. 17, Article ID 172302, 2003.

[7] K. Aamodt, E. L. Kryshen, R. Haake et al., "Suppression of charged particle production at large transverse momentum in central Pb-Pb collisions at $\sqrt{s_{NN}}$ = 2.76 TeV," *Physics Letters B*, vol. 696, no. 1-2, pp. 30–39, 2011.

[8] C. Adler, Z. Ahammed, C. Allgower et al., "Disappearance of back-to-back high pT hadron correlations in central Au+Au collisions at $\sqrt{s_{NN}}$ = 200 GeV," *Physical Review Letters*, vol. 90, no. 8, Article ID 082302, 2003.

[9] G. Aad, B. Abbott, J. Abdallah et al., "Observation of a centrality-dependent Dijet asymmetry in lead-lead collisions at $\sqrt{s_{NN}}$ = 2.76 TeV with the ATLAS detector at the LHC," *Physical Review Letters*, vol. 105, no. 25, Article ID 252303, 2010.

[10] S. Chatrchyan, V. Khachatryan, A. M. Sirunyan et al., "Observation and studies of jet quenching in PbPb collisions at $\sqrt{s_{NN}}$ = 2.76 TeV," *Physical Review C*, vol. 84, no. 2, Article ID 024906, 26 pages, 2011.

[11] CMS Collaboration, S. Chatrchyan et al., "Studies of jet quenching using isolated-photon+jet correlations in PbPb and pp collisions at $\sqrt{s_{NN}}$ = 2.76 TeV," *Physics Letters B*, vol. 718, no. 3, pp. 773–794, 2013.

[12] ATLAS Collaboration, "Measurement of the correlation of jets with high p_T isolated prompt photons in PbPb collisions at $\sqrt{s_{NN}}$ = 2.76 TeV with the ATLAS detector at the LHC," ATLAS-CONF-2012-121.

[13] S. Chatrchyan, V. Khachatryan, A. M. Sirunyan et al., "Measurement of jet fragmentation into charged particles in pp and PbPb collisions at $\sqrt{s_{NN}}$ = 2.76 TeV," *Journal of High Energy Physics*, vol. 2012, no. 10, article 76, 2012.

[14] CMS Collaboration, "Detailed Characterization of Jets in Heavy Ion Collisions Using Jet Shapes and Jet Fragmentation Functions," CMS-PAS-HIN-12-013.

[15] ATLAS Collaboration, "Measurement of inclusive jet charged-particle fragmentation functions in Pb+Pb collisions at $\sqrt{s_{\mathrm{NN}}}$ = 2.76 TeV with the ATLAS detector," *Physics Letters B*, 2014.

[16] S. Chatrchyan, V. Khachatryan, A. M. Sirunyan et al., "Modification of jet shapes in PbPb collisions at $\sqrt{s_{NN}}$ = 2.76 TeV," *Physics Letters B*, vol. 730, pp. 243–263, 2014.

[17] ATLAS Collaboration, G. Aad et al., "Measurement of the Azimuthal Angle Dependence of Inclusive Jet Yields in Pb+Pb Collisions at $\sqrt{s_{NN}}$ = 2.76 TeV with the ATLAS detector," *Physical Review Letters*, vol. 111, no. 15, Article ID 152301, 2013.

[18] A. Majumder, "A comparative study of jet-quenching schemes," *Journal of Physics G: Nuclear and Particle Physics*, vol. 34, no. 8, pp. S377–S387, 2007.

[19] J. Casalderrey-Solana and D. Teaney, "Transverse momentum broadening of a fast quark in a N = 4 Yang-Mills plasma," *Journal of High Energy Physics*, vol. 2007, no. 4, article 39, 2007.

[20] S. S. Gubser, S. S. Pufu, F. D. Rocha, and A. Yarom, "Energy loss in a strongly coupled thermal medium and the gauge-string duality," http://arxiv.org/abs/0902.4041.

[21] C. P. Herzog, A. Karch, P. Kovtun, C. Kozcaz, and L. G. Yaffe, "Energy loss of a heavy quark moving through N=4 supersymmetric Yang Mills Plasma," *Journal of High Energy Physics*, vol. 2006, no. 7, 2006.

[22] G.-L. Ma, "Dijet asymmetry in Pb+Pb collisions at $\sqrt{s_{NN}}$ = 2.76 TeV within a multiphase transport model," *Physical Review C*, vol. 87, no. 6, Article ID 064901, 2013.

[23] G.-L. Ma, "Towards detailed tomography of high energy heavy-ion collisions by γ-jet," *Physics Letters B: Nuclear, Elementary Particle and High-Energy Physics*, vol. 724, no. 4-5, pp. 278–282, 2013.

[24] G. L. Ma, "Decomposition of the jet fragmentation function in high-energy heavy-ion collisions," *Physical Review C*, vol. 88, no. 2, Article ID 021902, 2013.

[25] G.-L. Ma, "Medium modifications of jet shapes in Pb + Pb collisions at $\sqrt{s_{NN}}$ = 2.76 TeV within a multiphase transport model," *Physical Review C*, vol. 89, no. 2, Article ID 024902, 2014.

[26] M.-W. Nie and G.-L. Ma, "Azimuthal anisotropies of reconstructed jets in Pb+Pb collisions at $\sqrt{s_{\mathrm{NN}}}$ = 2.76 TeV in a multiphase transport model," *Physical Review C*, vol. 90, no. 1, Article ID 014907, 2014.

[27] Z.-W. Lin, C.-M. Ko, B.-A. Li, B. Zhang, and S. Pal, "A multi-phase transport model for relativistic heavy ion collisions," *Physical Review C*, vol. 72, no. 6, Article ID 064901, 2005.

[28] J. H. Chen, Y. G. Ma, G. L. Ma et al., "Elliptic flow of mesons and strange quark collectivity," *Physical Review C*, vol. 74, no. 6, Article ID 064902, 2006.

[29] B. Zhang, L.-W. Chen, and C.-M. Ko, "Charm elliptic flow at RHIC," *Physical Review C*, vol. 89, no. 2, Article ID 024906, 2005.

[30] G.-L. Ma and B. Zhang, "Effects of final state interactions on charge separation in relativistic heavy ion collisions," *Physics Letters, Section B: Nuclear, Elementary Particle and High-Energy Physics*, vol. 700, no. 1, pp. 39–43, 2011.

[31] G.-L. Ma and X.-N. Wang, "Jets, Mach cones, hot spots, ridges, harmonic flow, dihadron, and γ-hadron correlations in high-energy heavy-ion collisions," *Physical Review Letters*, vol. 106, no. 16, Article ID 162301, 2011.

[32] J. Xu, T. Song, C. M. Ko, and F. Li, "Elliptic flow splitting as a probe of the QCD phase structure at finite baryon chemical potential," *Physical Review Letters*, vol. 112, no. 1, Article ID 012301, 2014.

[33] C. M. Ko, L. W. Chen, V. Greco et al., "Mean-field effects on matter and antimatter elliptic flow," *Nuclear Science and Techniques*, vol. 24, no. 5, Article ID 050525, 2013.

[34] X.-N. Wang and M. Gyulassy, "Hijing: a Monte Carlo model for multiple jet production in pp, pA, and AA collisions," *Physical Review D*, vol. 44, no. 11, pp. 3501–3516, 1991.

[35] M. Gyulassy and X. N. Wang, "HIJING 1.0: a Monte Carlo program for parton and particle production in high energy hadronic and nuclear collisions," *Computer Physics Communications*, vol. 83, no. 2-3, pp. 307–331, 1994.

[36] B. Zhang, "ZPC 1.0.1: a parton cascade for ultrarelativistic heavy ion collisions," *Computer Physics Communications*, vol. 109, no. 2-3, pp. 193–206, 1998.

[37] B.-A. Li and C. M. Ko, "Formation of superdense hadronic matter in high energy heavy-ion collisions," *Physical Review C*, vol. 52, no. 4, pp. 2037–2063, 1995.

[38] J. Xu and C. M. Ko, "Pb-Pb collisions at $\sqrt{s_{NN}}$ = 2.76 TeV in a multiphase transport model," *Physical Review C: Nuclear Physics*, vol. 83, no. 3, Article ID 034904, 2011.

[39] J. Xu and C.-M. Ko, "Triangular flow in heavy ion collisions in a multiphase transport model," *Physical Review C*, vol. 84, no. 1, Article ID 014903, 2011.

[40] J. Xu and C. M. Ko, "Higher-order anisotropic flows and dihadron correlations in Pb-Pb collisions at $\sqrt{S_{NN}}$ = 2.76 TeV in a multiphase transport model," *Physical Review C: Nuclear Physics*, vol. 84, no. 4, Article ID 044907, 2011.

[41] T. Sjöstrand, P. Edén, C. Friberg et al., "High-energy-physics event generation with PYTHIA 6.1," *Computer Physics Communications*, vol. 135, no. 2, pp. 238–259, 2001.

[42] M. Cacciari, G. P. Salam, and G. Soyez, "FastJet user manual: (For version 3.0.2)," *European Physical Journal C*, vol. 72, no. 3, article 1896, pp. 1–54, 2012.

[43] I. Grabowska-Bold, "Measurement of isolated direct Photons in lead-lead collisions at $\sqrt{s_{NN}}$ = 2.76 TeV with the ATLAS detector," *Nuclear Physics A*, vol. 904-905, pp. 577c–580c, 2013.

[44] S. Chatrchyan, V. Khachatryan, A. M. Sirunyan et al., "Measurement of isolated photon production in *pp* and PbPb collisions at $\sqrt{s_{NN}}$ = 2.76 TeV," *Physics Letters B*, vol. 710, no. 2, pp. 256–277, 2012.

[45] V. Greco, C. M. Ko, and P. Lévai, "Partonic coalescence in relativistic heavy ion collisions," *Physical Review C—Nuclear Physics*, vol. 68, no. 3, Article ID 034904, 2003.

[46] T. Renk and K. J. Eskola, "Proton-antiproton suppression in 200A GeV Au-Au collisions," *Physical Review C*, vol. 76, no. 2, Article ID 027901, 2007.

[47] B. Alver and G. Roland, "Collision-geometry fluctuations and triangular flow in heavy-ion collisions," *Physical Review C*, vol. 81, no. 5, Article ID 054905, 2010.

[48] B. Alver and G. Roland, "Erratum: collision-geometry fluctuations and triangular flow in heavy-ion collisions [Phys. Rev. C 81, 054905 (2010)]," *Physical Review C*, vol. 82, no. 3, Article ID 039903, 1 page, 2010.

[49] L. X. Han, G. L. Ma, Y. G. Ma et al., "Initial fluctuation effect on harmonic flows in high-energy heavy-ion collisions," *Physical Review C: Nuclear Physics*, vol. 84, no. 6, Article ID 064907, 2011.

[50] M. Gyulassy, I. Vitev, and X.-N. Wang, "High *PT* azimuthal asymmetry in noncentral $A + A$ at RHIC," *Physical Review Letters*, vol. 86, no. 12, pp. 2537–2540, 2001.

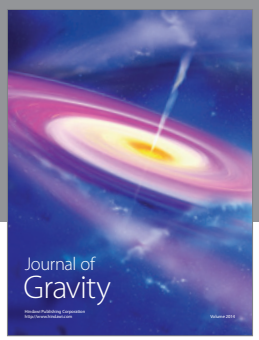

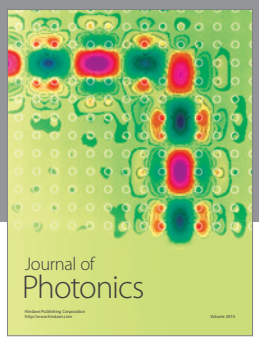

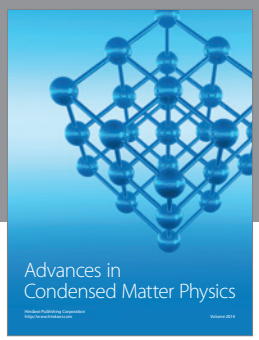

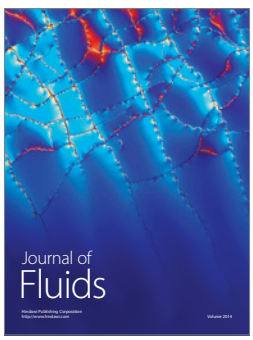

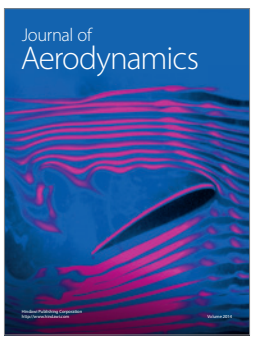

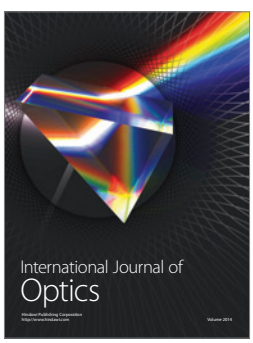

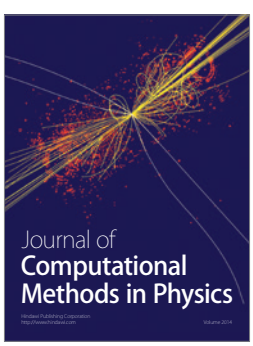

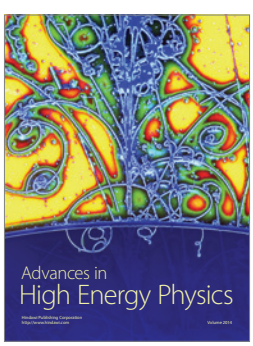

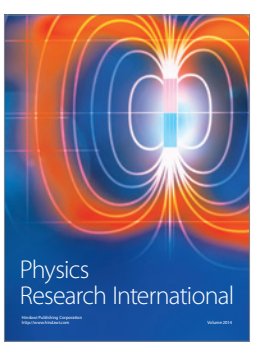

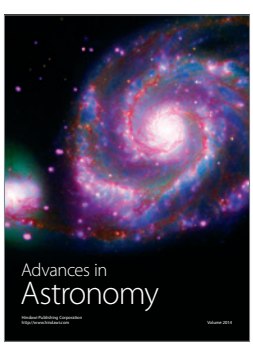

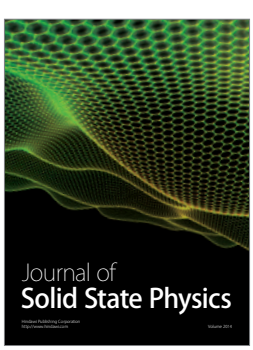

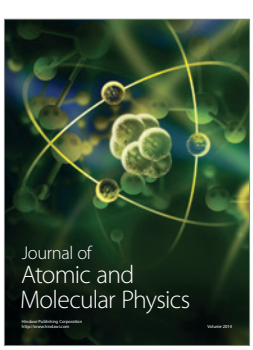

Hindawi

Submit your manuscripts at
http://www.hindawi.com